A STUDY OF SHEAR LAYER SUB-STRUCTURES IN LEADING EDGE VORTICES USING LASER DOPPLER VELOCIMETRY

Joshua D. Butler*
***Clarkson University, Potsdam, NY**

Abstract

Non-intrusive Laser Doppler Velocimetry measurements were taken of leading edge vortices about a 70^o and 80^o, flat plate delta wing. Periodic and stationary instabilities within the shear layer have been reported in literature. This study was initiated in an attempt to quantify the characteristics of these substructures as a function of leading edge sweep, angle of attack, and chord-wise position to better understand the complex physics of this three-dimensional aerodynamic phenomenon. Through these experiments, one- and two-dimensional plots of velocity components, turbulence intensity, and vorticity were analyzed. These results show evidence of the state of the vortex strength with respect to the leading edge sweep (Λ), angle of attack (α), and chord-wise position (x/C) and correlate it to the magnitude of the turbulence intensity present within the shear layer of the forced vortex.

Nomenclature

C	=	chord length
s^*	=	local semi-span
u	=	x-component (axial) velocity
U_∞	=	free stream velocity
v	=	y-component velocity
w	=	z-component velocity
x/C	=	chord-wise position
α	=	angle of attack
Λ	=	leading edge sweep
Θ	=	elevation angle of vortex core
Ω	=	axial vorticity
Ψ	=	outboard angle of vortex core

1 Introduction

Recent numerical studies of the vortices generated by highly swept delta wings [1,2] have supported previous observations and measurements of the existence of spatially stationary sub-structures in the shear layer [3-7]. The goal of this investigation was to obtain detailed data of these sub-structures using a non-intrusive measurement technique. The location of the vortex core has been shown to be displaced with the presence of a probe in the flow and a non-intrusive technique could provide data truer to that of the naturally evolving vortex [8]. This data may be used to provide physical concepts of the internal makeup of the shear layer to present a better understanding of the evolution of leading edge vortices.

2 Background

As the attached flow on windward pressure surface of the delta wing moves outboard towards the leading edge, it encounters a sharp discontinuity that causes the flow to separate and form a sheet of vorticity. The local pressure gradient causes the sheet to rotate into a tight spiral known as the primary vortex. A portion of the encountered free stream flows over the apex of the wing and is temporarily attached to the suction surface. This flow is drawn in the span-wise direction towards the leading edge by the primary vortex. The pressure gradient associated with the shear layer at the leading edge causes the suction surface flow to separate from the plate and form a secondary vortex that rotates in the

opposite direction to that of the primary vortex. This flow field is illustrated in Figure 2 [8].

Fig. 1. Flow visualization of spatially stationary sub-structures (Payne, Ng, and Nelson [14]).

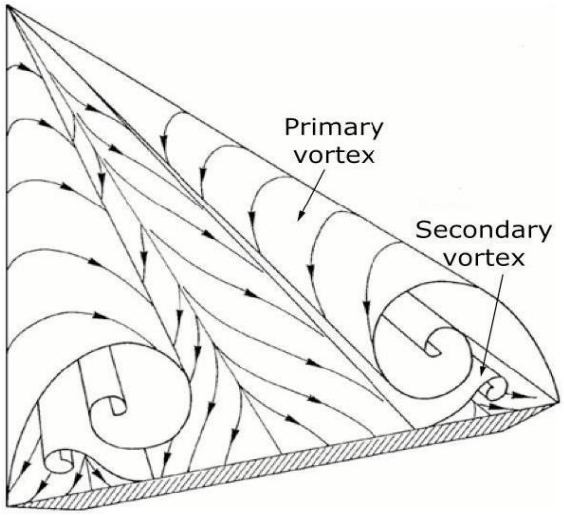

Fig. 2. Schematic of flow about a delta wing (Delery [8]).

Leading edge vortices increase in strength as the angle of attack increases and decrease in strength as the distance from the apex to the trailing edge increases until they approach breakdown. They induce a low pressure zone on the upper surface of the wing that creates a nonlinear lift-curve. The secondary vortex displaces the primary vortex upwards and inboard. This effect is greater if the upper surface boundary layer is laminar because the shear layer separates at a more inboard position creating a larger secondary vortex. Near the leading edge, the flow separates again and joins the flow in the lower surface of the shear layer.

Two types of instabilities have been observed throughout the evolution of the vortex and many of these studies can be found in Reference 9. The first has been considered a quasi-periodic inviscid instability that forms relatively parallel to the leading edge [10-13]. The second is a spatially stationary vortex cell that rotates in the same direction as the primary vortex. Several of these cells may be observed within the shear layer at any plane perpendicular to the rotation axis of the vortex core. Figure 1 illustrates a laser light sheet of one such plane [14]. The structures have also been observed with flow field measurements shown in Figure 3 [6]. As the vortex evolves downstream, the sub-structures tend to become less distinct.

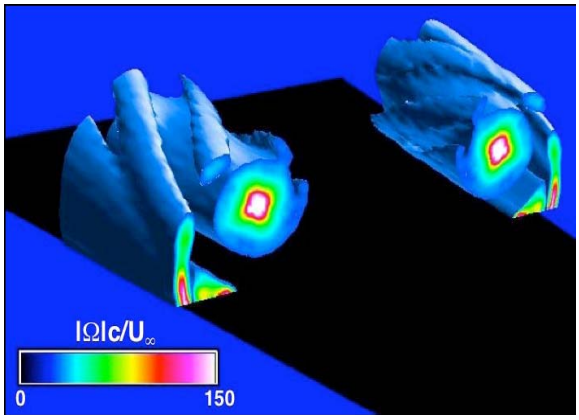

Fig. 3. Iso-vorticity surfaces, $0.70 \leq x/c \leq 0.80$ on an 80^{o} delta wing at $\alpha = 15^{o}$ (Washburn and Visser [6]).

The development of the shear layer and sub-structures has been observed to be boundary layer dependent. The shear layer characteristics change when the upper surface boundary layer is turbulent. A turbulent boundary layer may create a thicker shear layer. If true, this concept could be used to manipulate the location of breakdown. The ability to control the size and strength of the vortex may allow for reduced drag at cruising conditions or increased lift during high angle of attack scenarios.

3 Experimental Overview

Wind tunnel experiments were done in the Clarkson University subsonic, particle wind tunnel. The tunnel is an open circuit type with a 9:1 inlet contraction. The test section is 48 inches by 36 inches and is powered by a 20 HP, 3-phase frequency driven motor with a 10-bladed fan. A honeycomb grate and fine screens are added to the inlet to reduce turbulence and flow irregularities. The maximum speed of this tunnel is approximately 18 m/s creating a *Re* of about 1.18e06/m at the test section. Since LDV requires a particulate to scatter the laser light, flow quality was studied to test uniformity and turbulence before and after the particle injection system was added.

The delta wing models were flat plates 6.125 mm thick with a sharp leading edge bevel and Λ's of 70^o and 80^o. The leading edge bevel allows for a distinct vortex sheet formation that is virtually Reynolds number independent.

Flow visualization and three-component LDV measurements were used for a parametric study of each wing at multiple angles of attack and several chord-wise locations. The choice of LDV allowed for non-intrusive data acquisition in an effort to minimize adverse effects on the natural evolution of the vortex. Setup of the system involved mounting a three-axis TSI traverse to the ceiling rafters above the test section, assembly of the LDV hardware components, positioning of the system for ideal data acquisition, optimization of laser power efficiency, and a critical beam alignment process that ensured each beam component coincided on a particular point in space.

4 Results

Two-dimensional sets of three-component flow field data were acquired. These tests were acquired parallel to the trailing edge and perpendicular to the core's elevation angle Θ as shown in Figure 4. All data was processed to display values in a Cartesian coordinate system relative to the vortex core's rotational axis where Θ and Ψ were determined by surface flow visualization and a series of Pitot-static tube tests about the vortex. Values analyzed in this investigation include velocity components, turbulence intensities, and vorticity. All values were normalized with the local semi-span, *s**, and/or the free stream velocity, U_∞, when appropriate.

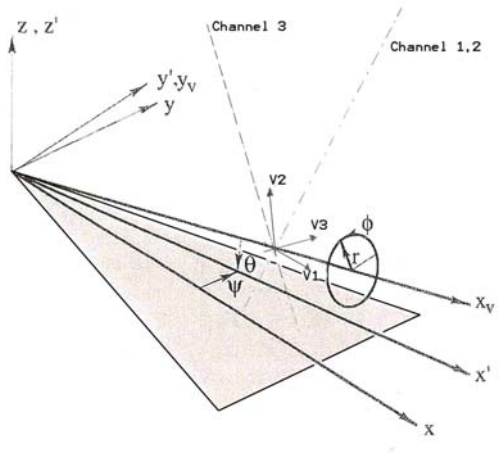

Fig. 4. Components of raw LDV data relative to vortex core.

4.1 Two-Dimensional Data

Figures 5-10 display planar maps of axial velocity. These figures show that as α increased, axial velocity increased for a given *x/C* and Λ. There was a minimal change in axial velocity as *x/C* increased from .43 to .50 as shown in Figures 8 and 9 for Λ=80^o and α=15^o. This is because the increasing characteristics of the vortex scale linearly with *s** for a certain range of *x/C* values dependant on α and Λ just before the vortex loses rotational strength and breaks down. These results also show that higher values of Λ produce lower values of axial velocity. Higher values of axial velocity correspond to stronger vortices because the stronger rotation of the vortex induces a lower pressure near the vortex core which accelerates flow axially along the core.

Figure 6 shows a value of zero for axial velocity near the vortex core. This value was caused by an absence of data obtained at that location due to the presence of few particles in and near the core. The dispersion of particles in a vortex is shown in Figure 7 from the test results of Λ=70°, α=20°, and x/C=0.43. This figure shows a relatively high existence of particles within the shear layer and ambient flow and a relatively low quantity near the free vortex core. Statistical studies were performed from data sets such as this in order to establish validity of the results.

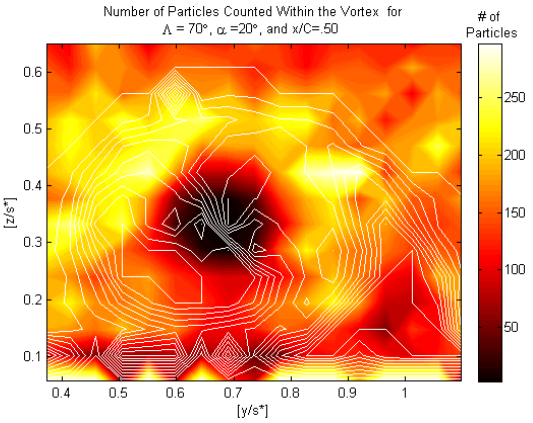

Fig. 7. Particle count within a vortex at 9.71 m/s.

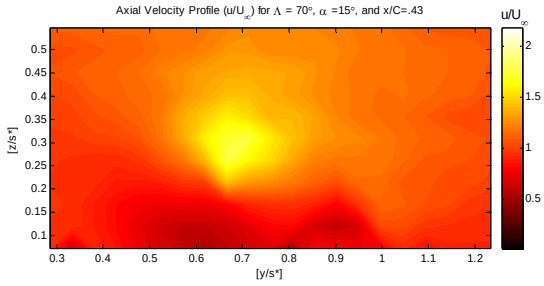

Fig. 5. Axial velocity map, % u/U_∞, Λ=70°, α=15°, x/C=.43 at 9.74 m/s.

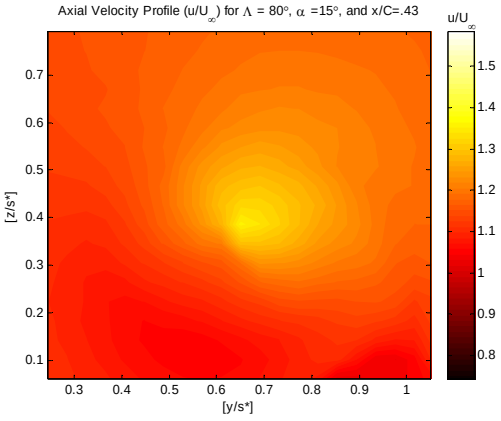

Fig. 8. Axial velocity map, % u/U_∞, Λ=80°, α=15°, x/C=.43 at 9.81 m/s.

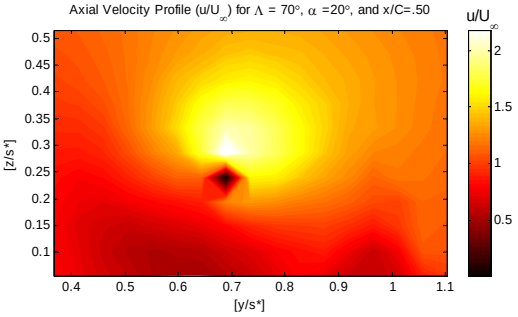

Fig. 6. Axial velocity map, % u/U_∞, Λ=70°, α=20°, x/C=.50 at 9.71 m/s.

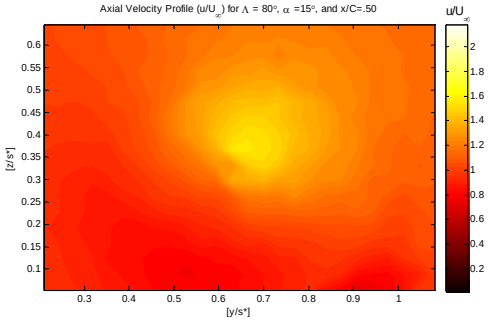

Fig. 9. Axial velocity map, % u/U_∞, Λ=80°, α=15°, x/C=.50 at 9.80 m/s.

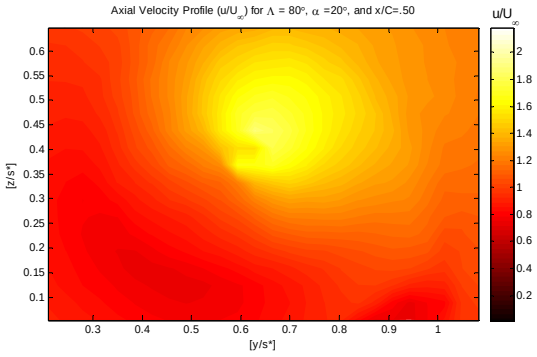

Fig. 10. Axial velocity map, % u/U_∞, Λ=80°, α=20°, x/C=.50 at 9.69 m/s.

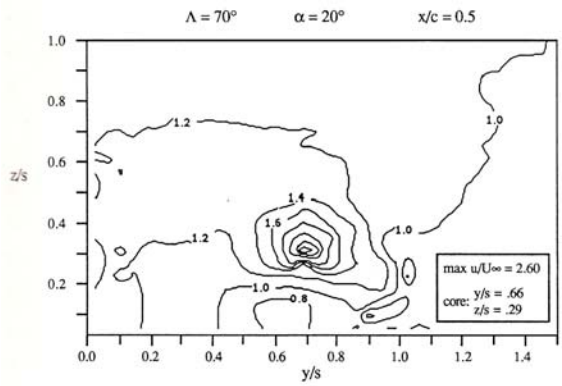

Fig. 11. Axial velocity map obtained with seven-hole probe, Visser [8].

Figures 11 and 12 show a comparison of seven-hole probe data acquired by Visser and LDV data. The LDV data shows a value of axial velocity of 2.1. When compared to Visser's 2.6, the LDV data is approximately 20% lower. This may be due to the grid resolution not capturing the characteristics of the high velocity gradient near the vortex core.

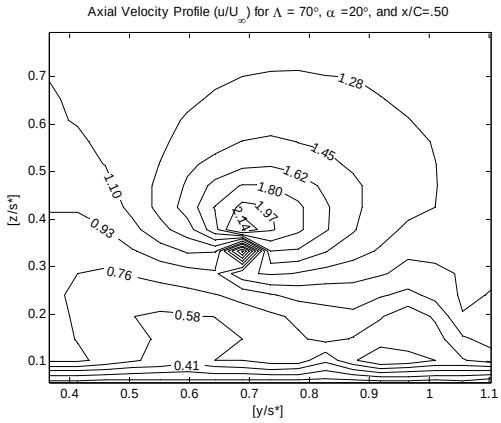

Fig. 12. Axial velocity map obtained with LDV.

Figures 13-23 show results of v- and w-component velocities. These results reveal similar characteristics as the axial velocity results; as α increased, the values of v and w increased. It is also shown that as Λ increased, the values of v and w decreased. When comparing Figures 16 and 17, the vertical velocity component, w increased as α increased from 15° to 20° for Λ=80° and x/C=.50 indicating an increase in the strength of the vortex.

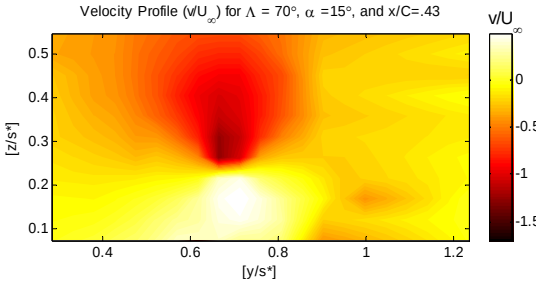

Fig. 13. v-velocity map, % v/U_∞, Λ=70°, α=15°, x/C=.43 at 9.71 m/s.

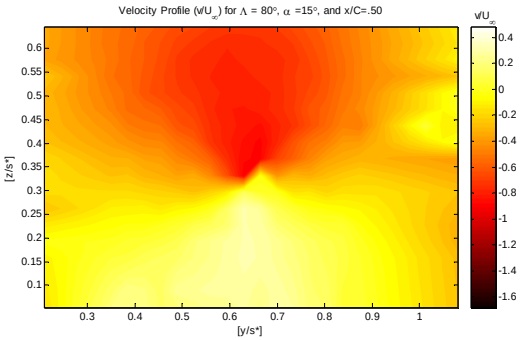

Fig. 16. v-velocity map, % v/U_∞, Λ=80°, α=15°, x/C=.50 at 9.80 m/s.

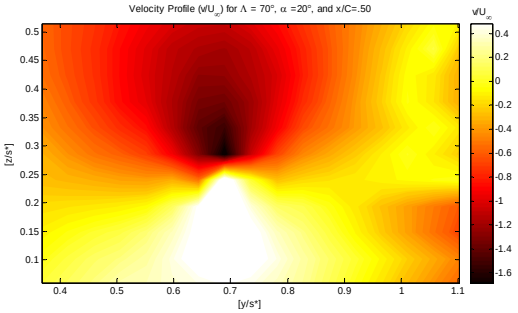

Fig. 14. v-velocity map, % v/U_∞, Λ=70°, α=20°, x/C=.50 at 9.84 m/s.

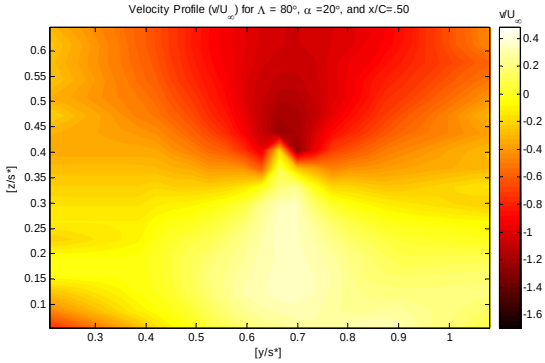

Fig. 17. v-velocity map, % v/U_∞, Λ=80°, α=20°, x/C=.50 at 9.69 m/s.

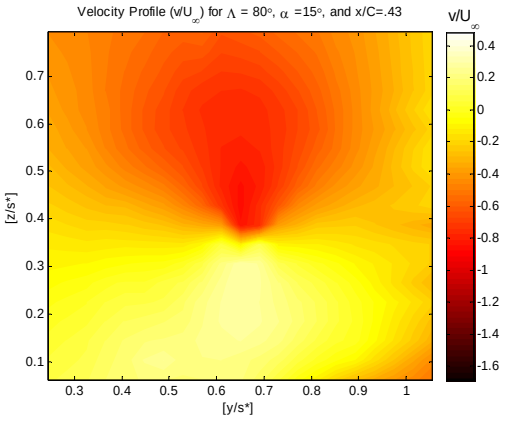

Fig. 15. v-velocity map, % v/U_∞, Λ=80°, α=15°, x/C=.43 at 9.81 m/s.

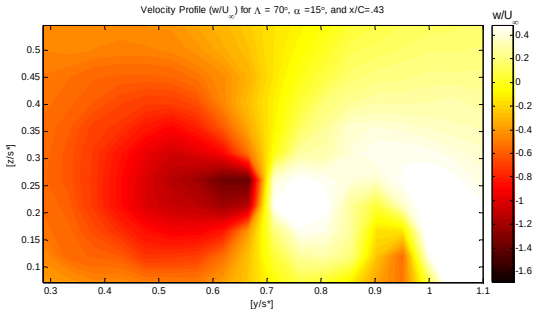

Fig. 18. w-velocity map, % w/U_∞, Λ=70°, α=15°, x/C=.43 at 9.71 m/s.

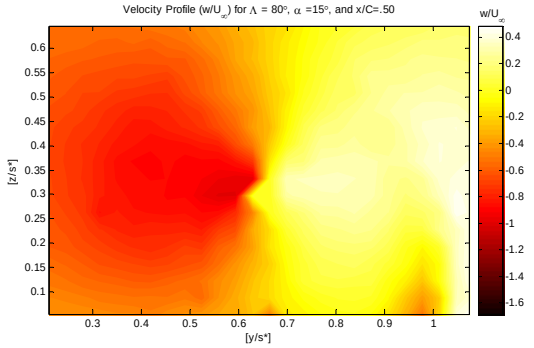

Fig. 21. w-velocity map, % w/U_∞, Λ=80°, α=15°, x/C=.50 at 9.80 m/s.

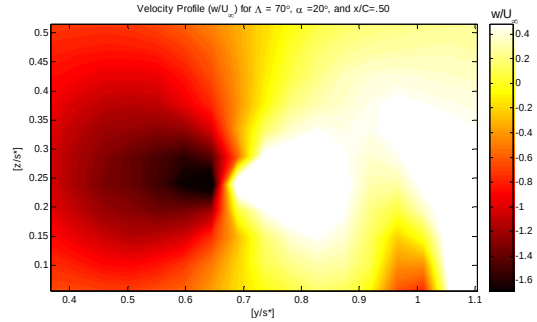

Fig. 19. w-velocity map, % w/U_∞, Λ=70°, α=20°, x/C=.50 at 9.84 m/s.

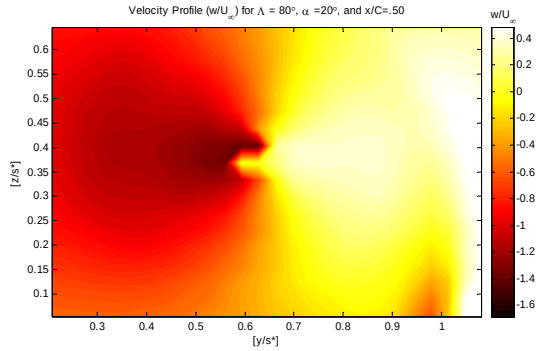

Fig. 22. w-velocity map, % w/U_∞, Λ=80°, α=20°, x/C=.50 at 9.69 m/s.

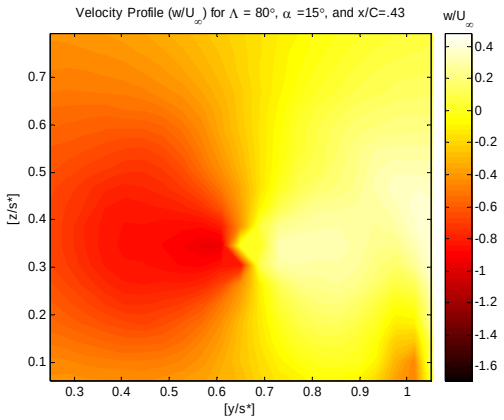

Fig. 20. w-velocity map, % w/U_∞, Λ=80°, α=15°, x/C=.43 at 9.81 m/s.

Figures 23-27 display axial turbulence intensity within the shear layer. The values of turbulence intensity were calculated by the average of the fluctuations from the mean local velocity, u. The difference from those two values was then normalized by the local velocity, u and presented as a percentage. These results were then processed to determine the turbulence intensity fluctuations with respect to the free stream velocity, U_∞.

These figures show that as the angle of attack increased for a given Λ and x/C the turbulence intensity increased as shown in Figures 26 and 27. As the leading edge sweep, Λ increased from 70° to 80°, it was found that the turbulence intensity within the shear layer decreased as shown in Figures 24 and 27 respectively. The results from the axial

turbulence intensity plots show that parameters that produce higher strength vortices produce higher values of axial turbulence intensity in the shear layer.

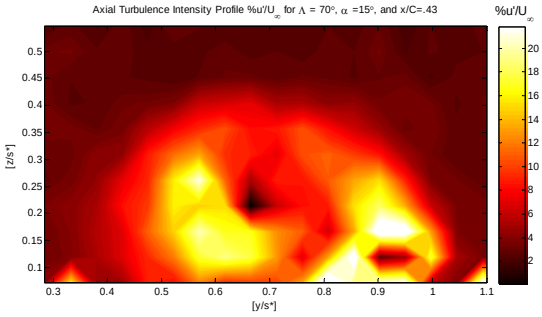

Fig. 23. Axial turbulence intensity, % *u*'/U_∞, Λ=70°, α=15°, *x/C*=.43 at 9.71 m/s.

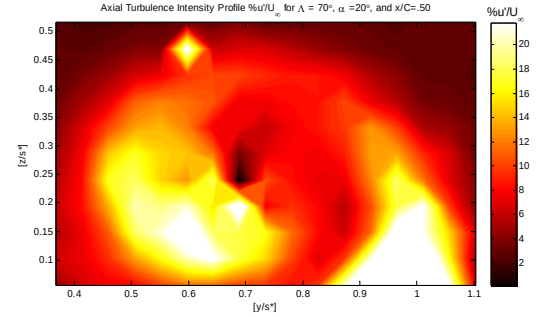

Fig. 24. Axial turbulence intensity, % *u*'/U_∞, Λ=70°, α=20°, *x/C*=.50 at 9.84 m/s.

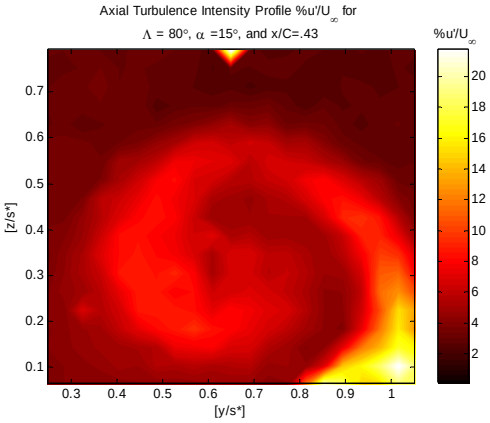

Fig. 25. Axial turbulence intensity, % *u*'/U_∞, Λ=80°, α=15°, *x/C*=.43 at 9.81 m/s.

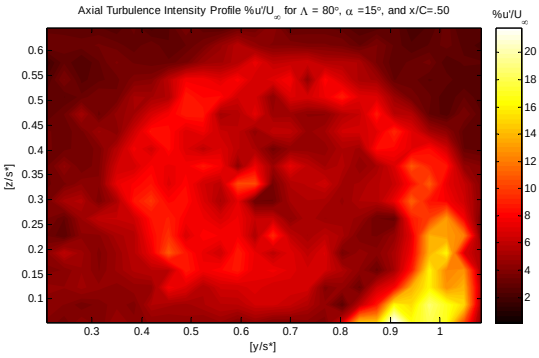

Fig. 26. Axial turbulence intensity, % *u*'/U_∞, Λ=80°, α=15°, *x/C*=.50 at 9.80 m/s.

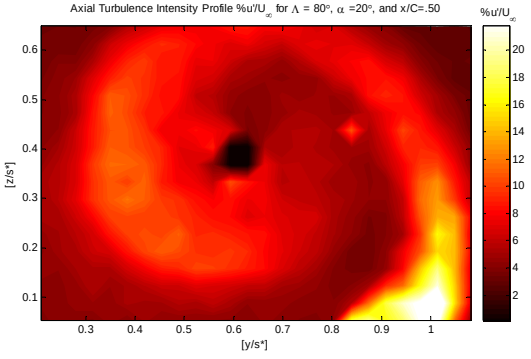

Fig. 27. Axial turbulence intensity, % *u*'/U_∞, Λ=80°, α=20°, *x/C*=.50 at 9.69 m/s.

Axial vorticity plots represent the local strength of the vortex and are shown in Figures 28-33. These values were calculated from the *v*- and *w*-components of velocity and the data grid spacing of each test. This was done by dividing the change of velocity from one grid point to the next by the physical grid spacing between those two points. Figures 30 and 31 show a relatively constant value of vorticity as *x/C* increase from 0.43 to 0.50 for α=15^o and Λ=80. An increase in vorticity from $\Omega_x s^*/U_\infty$=60 to 80 can also be seen from Figures 31 to 32 as α increased from 15 to 20^o for Λ=80^o. Figure 33 represents the same test case as Figure 32, however the high magnitude of axial vorticity near the core has been omitted to show the characteristics of the vorticity within the shear layer. Ambient and core values have been filtered out of this plot and the shear layer reveals relatively weak, co-rotating vorticity cells that are an order of magnitude lower than the vortex core.

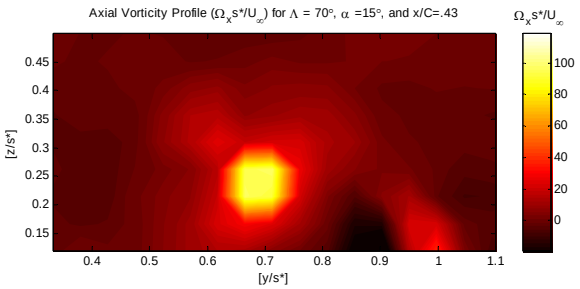

Fig. 28. Axial vorticity, $\Omega_x s^*/U_\infty$, Λ=70^o, α=15^o, *x/C*=.43 at 9.71 m/s.

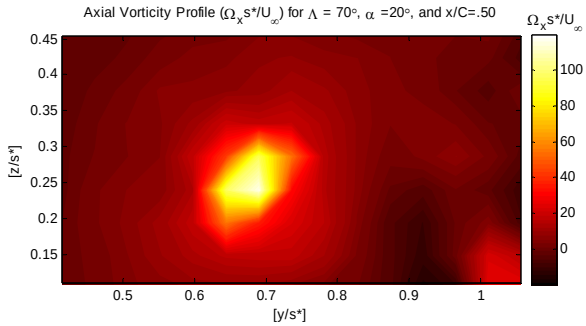

Fig. 29. Axial vorticity, $\Omega_x s^*/U_\infty$, Λ=70^o, α=20^o, *x/C*=.50 at 9.84 m/s.

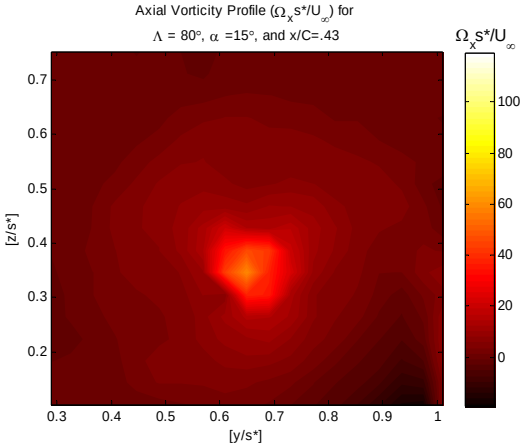

Fig. 30. Axial vorticity, $\Omega_x s^*/U_\infty$, Λ=80^o, α=15^o, *x/C*=.43 at 9.81 m/s.

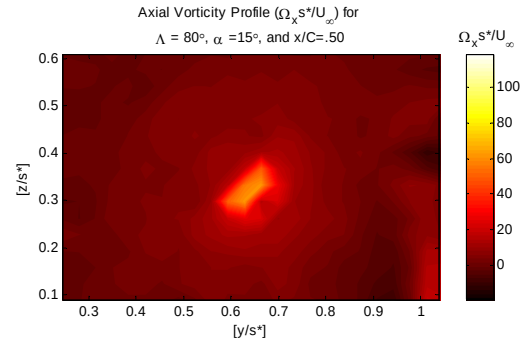

Fig. 31. Axial vorticity, $\Omega_x s^*/U_\infty$, Λ=80^o, α=15^o, *x/C*=.50 at 9.80 m/s.

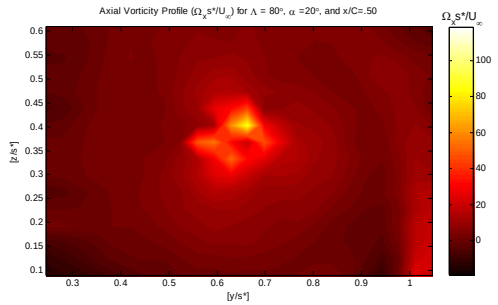

Fig. 32. Axial vorticity, $\Omega_x s^*/U_\infty$, Λ=80^o, α=20^o, *x/C*=.50 at 9.69 m/s.

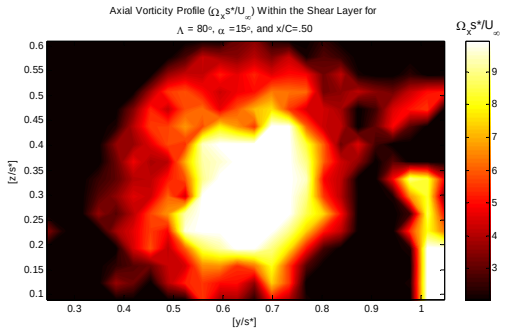

Fig. 33. Axial vorticity within the shear layer, $\Omega_x s^*/U_\infty$, Λ=80°, α=15°, x/C=.50 at 9.80 m/s.

5 Conclusion

A series of measurements has been acquired using Laser Doppler Velocimetry over two delta wings. Velocity measurements and turbulence intensities were recorded for a series of angles of attack from 10° to 15° at wind tunnel velocities between 9.5 and 10.0 m/s.

The characteristics of axial turbulence intensity have provided evidence of the contribution of the shear layer to the evolution of the vortex. As the angle of attack, α increases, breakdown occurs closer to the apex and axial turbulence intensity has been found to increase within the shear layer. The vortex also gained strength as x/C increased at a given angle of attack, α. For these conditions, axial turbulence intensity within the shear layer also increased. Higher values of leading edge sweep, Λ created weaker vortices and weaker values of axial turbulence intensity were observed in the shear layer. This data shows evidence that stronger vortices have higher values of axial turbulence intensity within the shear layer and that perhaps the onset of vortex breakdown may be triggered by such an increase in turbulence within the shear layer. This is also supported by increased values of axial vorticity of the vortex core being related to higher values of turbulence intensity in the shear layer. It may be possible that values of turbulence intensity, or turbulent kinetic energy may be present at the onset of vortex breakdown.

Use of LDV does show promise for delta wing experiments as a non-intrusive technique however it is time consuming. Other systems such as Particle Imaging Velocimetry [PIV] may be easier to acquire data of instantaneous vortex characteristics. A PIV system's ability to capture a field of data would be more desirable with respect to acquisition time, particle and spray material consumption and possible spectral analysis of sub-structure cells. However, PIV acquires data within a very short time span and more particles may be necessary to achieve quality data.

References

[1] Mitchell A. M., Molton P. and Forsythe J., "Analysis of Delta Wing Vortical Substructures Using Detached- Eddy Simulation," AIAA Paper 2002-2968.

[2] Visbal M. R. and Gordnier R. E.,"On the Structure of the Shear Layer Emanating from a Swept Leading Edge at Angle of Attack," AIAA Paper 2003-4016, June 2003.

[3] Payne F. M., Ng T. T. and Nelson R. C., "Visualisation and Wake surveys of Vortical Flow over a Delta Wing," AIAAJournal, Vol.26 No.2, February 1988, pp. 137-143.

[4] Campbell, J. F. and Chambers, J. R., "Patterns in the Sky, Natural Visualization of Aircraft Flow Fields", NASA SP-514,NASA Langley research Center, 1994.

[5] Verhaagen, N. G.; Meader, J. P.; and Verhelst, J. M.: "Boundary Layer Effects on the Flow of a Leading Edge Vortex",AIAA-93-3463-CP, Aug. 1993.

[6] Washburn A. E. and Visser K. D.,"Evolution of Vortical Structures in the Shear Layer of Delta Wings" AIAA Paper 1994-2317, June 1994.

[7] Honkan A. and Andreopouloulos J. "Instantaneous Three-Dimensional Vorticity Measurements in Vortical Flow over aDelta Wing"} AIAA Journal, Vol. 35 No. 10, October 1997, pp 1612-1620.

[8] Delery J. M. "Robert Legendre and Henri Werle : Toward the Elucidation of Three-Dimentional Separation" Annual Review of Fluid Mechanics, Vol.33, 2001.

[9] Visser, K.D., Ferrero Ferrero, M. del Carmen, and Nelson, R.C., "Physical Considerations of Leading Edge Flows," AIAA 2004-5083, 22nd Applied

Aerodynamics Conference, Providence, RI, August 2004.
[10] Gad-el-Hak, M. and Blackwelder, R. F.: “The Discrete Vortices from a Delta Wing”, AIAA Journal, Vol. 23, No. 6, 1985.
[11] Reynolds, G. A. and Abtahi,: “Three-Dimensional Vortex Development, Breakdown, and Control”, AIAA89-0998.
[12] Lowson, M. V.: “The Three Dimensional Vortex Sheet Structure on Delta Wings”, Fluid Dynamics of Three DimensionalTurbulent Shear Flows and Transition, AGARD-CP-438, Paper 11, 1988.
[13] Riley A. J. and Lowson M. V.,"Development of a Three-dimensional Free Shear Layer,” Journal of Fluid Mechanics, Vol.369, pp.49-89, 1998, pp 49-89.
[14] Payne F. M., Ng T. T. and Nelson R. C., "Experimental Study of the Velocity Field on a Delta Wing" AIAA Paper 1987-1231, June 1987.
[15] Campbell, J. F. and Chambers, J. R., “Patterns in the Sky, Natural Visualization of Aircraft Flow Fields”, NASA SP-514, NASA Langley research Center, 1994.

Copyright Statement

The authors confirm that they, and/or their company or institution, hold copyright on all of the original material included in their paper. They also confirm they have obtained permission, from the copyright holder of any third party material included in their paper, to publish it as part of their paper. The authors grant full permission for the publication and distribution of their paper as part of the ICAS2008 proceedings or as individual off prints from the proceedings.